Nano Research
DOI 10.1007/s12274-016-1264-x
Research Article
ISSN 1998-0124
CN 11-5974/O4

In situ synthesis of graphene oxide/gold nanorods theranostic hybrids for efficient tumor computed tomography imaging and photothermal therapy

Bingmei Sun[1,2], Jinrui Wu[3], Shaobin Cui[2], Huanhuan Zhu[2], Wei An[3], Qingge Fu[4], Chengwei Shao[5], Aihua Yao[1] (✉), Bingdi Chen[2] (✉), and Donglu Shi[2,6]

[1] *School of Materials Science and Engineering, Tongji University, Caoan Road 4800, Shanghai 201804, China*
[2] *The Institute for Translational Nanomedicine, Shanghai East Hospital, The Institute for Biomedical Engineering & Nano Science, Tongji University School of Medicine, Shanghai 200120, China*
[3] *School of Mechanical Engineering, Tongji University, Shanghai 200092, China*
[4] *Department of Emergency, Changhai Hospital, Second Military Medical University, Shanghai 200433, China*
[5] *Radiology Department of Changhai Hosptial, Second Military Medical University, Shanghai 200433, China*
[6] *Materials Science and Engineering Program, Department of Mechanical and Materials Engineering, College of Engineering and Applied Science, University of Cincinnati, Cincinnati, Ohio 45221-0012, USA*

Received: 22 June 2016
Revised: 12 August 2016
Accepted: 26 August 2016

KEYWORDS
graphene oxide/gold nanorods,
in situ growth,
computed tomography imaging,
photothermal therapy

ABSTRACT

Graphene oxide/gold nanorod (GO/GNR) nanohybrids were synthesized with a GO- and gold-seed-mediated *in situ* growth method at room temperature by mixing polystyrene sulfonate (PSS) functionalized GO, secondary growth solution, and gold seeds. Compared with *ex situ* preparation methods of GO/GNRs or graphene (G)/GNRs, the *in situ* synthesis of GO/GNRs addressed the issue of the aggregation of the GNRs before their attachment onto the GO. The method is straightforward and environment-friendly. The GO/GNRs showed a remarkable photothermal effect *in vitro*. The temperature of the GO/GNR nanohybrids increased from 25 to 49.9 ℃ at a concentration of 50 μg/mL after irradiation with an 808-nm laser (0.4 W/cm^2) for 6 min. Additionally, the GO/GNRs exhibited good optical and morphological stability and photothermal properties after six cycles of laser irradiation. Upon injection of the GO/GNRs into xenograft tumors, excellent computed tomography (CT) imaging properties and photothermal effect were obtained. The preclinical CT agent iohexol was combined with the GO/GNRs and further enhanced CT imaging. Therefore, the GO/GNR nanohybrids have great potential for precise CT-image-guided tumor photothermal treatment.

Address correspondence to Aihua Yao, aihyao@126.com; Bingdi Chen, inanochen@tongji.edu.cn

1 Introduction

Photothermal therapy (PTT), which typically involves the conversion of absorbed light into local heating to kill cancer cells or tissues [1–5], is one of the most attractive methods for tumor ablation and regression. One of the advantages of PTT is that near-infrared light (NIR) does little damage normal biological tissues [1]. Compared with chemotherapy and radioactive therapy, PTT also offers the benefits of short treatment, noninvasiveness without bleeding, and absence of physical side-effects. The NIR absorption of gold nanorods (GNRs) can be adjusted by changing the aspect ratio of the GNRs [6, 7]. GNRs could be used in drug or gene delivery [8, 9], biosensing [10, 11], and medical diagnosis [8, 12–14]. Additionally, GNRs are potential imaging contrast agents employed in positron emission tomography [8], photoacoustic [12], and computed tomography (CT). Among these, CT imaging is based on the high atomic number and X-ray absorption coefficient [15–18] of gold. Considering their strong photothermal effect, GNRs could be used in imaging-guided tumor PTT. Despite the advantages of GNRs, the aggregation of GNRs presents challenges regarding the improvement of photoconversion and CT imaging.

GNRs can be conjugated onto two-dimensional (2D) nanostructures, such as graphene (G), graphene oxide (GO), and reduced GO, for various functionalities and utilized in PTT [19–21] and drug or gene delivery [19, 22–25]. It is worth mentioning that GNRs grown on G or its derivatives have also been investigated for PTT [26–30]. Gold nanorods grown *in situ* on GO could increase the large surface area of GO/GNRs to the benefit of being a carrier. To synthesize multifunctional G/gold nanoparticles (NPs), Abdallah et al. [26] combined gold NPs with GO using laser irradiation. In this process, however, the GO was reduced after the laser irradiation. Gil et al. [31] explored the role of oxygen moieties on the surface of G in gold nucleation and prepared G/gold NPs. Based on this result, we hypothesize that gold seeds could be successfully grown into GNRs on functional G or GO. Similarly to G, GO is known to have many oxygen-containing functional groups, which make it more soluble and biocompatible and, therefore, an ideal template for GNRs. Several nanosystems containing G or GO have been developed based on gold [26, 31–34], Ag [35–37], Cu_2O [38], and CuS [39] NPs. A previous study conducted by our group investigated the *in situ* preparation of cobalt oxide quantum dot/G nanosheet hybrids [40] and is the foundation for this work. Here, a GO- and gold-seed-mediated *in situ* growth method was developed to stabilize GNRs and overcome severe aggregation. The method is environmentally benign and straightforward.

GO/GNR nanohybrids were synthesized by mixing GO-polystyrene sulfonate (PSS), a secondary growth solution, and gold seeds. The gold seeds produced GNRs on the GO-PSS substrate rapidly but also stably and uniformly. The GO/GNRs exhibited excellent CT imaging properties and photothermal effect both *in vitro* and *in vivo*. The photothermal stability of the GO/GNRs was determined to be good after six cycles of 808-nm laser irradiation. The GO/GNRs were synthesized for the first time by using this GO- and gold-seed-mediated *in situ* growth method and were shown to be a promising candidate for precise CT-image-guided tumor PTT.

2 Experimental

2.1 Materials

Graphite flakes (nature, −10 mesh) and PSS (M_W = 70,000) were purchased from Alfa Aesar (Tianjin, China). Phosphoric acid, sulfuric acid, hydrochloric acid, hydrogen peroxide, potassium permanganate, and silver nitrate were obtained from Sinopharm Chemical Reagent Beijing Co., Ltd. (Beijing, China). Hexadecyl trimethyl ammonium bromide, sodium borohydride, ascorbic acid, and poly(diallyl ammonium chloride) (PDDAC) (M_W = 100,000–200,000) were acquired from Sigma (Shanghai, China) and $HAuCl_4{\cdot}4H_2O$ was obtained from Beijing HWRK Co., Ltd. (Beijing, China). The commercial CT contrast agent iohexol was provided by Changhai Hospital (Shanghai, China).

2.2 Preparation and noncovalent modification of GO

GO was synthesized as previously reported [41]. The modification process of the GO was as follows: First,

0.8 g of PSS was dispersed in 60 mL of deionized water; then, 10 mg of dried GO were added into the PSS solution, and the mixed solution was sonicated (880 W, 10 min). To remove the excess PSS, the mixed solution was purified with three cycles of centrifugation at 11,000 rpm for 20 min and redispersed in 20 mL of deionized water.

2.3 Preparation and modification of GO/GNR nanohybrids

GO/GNRs were synthesized in an aqueous cetyltrimethylammonium bromide (CTAB) solution by using a seed-mediated growth method [6]. The gold seeds were prepared by mixing $HAuCl_4{\cdot}4H_2O$ (1.0 M, 1.5 mL) with CTAB (0.2 M, 2.5 mL). Then, freshly prepared ice-cold $NaBH_4$ (0.01 M, 600 μL) was added and incubated at 25 ℃ for 2 h. Subsequently, the growth solution was prepared by adding $HAuCl_4{\cdot}4H_2O$ (24 mM, 3.125 mL) to the CTAB (0.02 M, 50 mL) solution. Next, 20 mL of GO (~0.5 g/mL), $AgNO_3$ (4 mM, 2.8 mL) and ascorbic acid (0.08 M, 1.25 mL) were introduced into the solution. Subsequently, 1 mL of the gold seed solution was added into the growth solution and maintained at 28 ℃ overnight. The final solution was purified with deionized water by three centrifugation cycles and redispersed in 30 mL of deionized water. Then, approximately 0.6 g of PSS was introduced into 30 mL of the GO/GNR solution and the mixture was sonicated (100 W, 30 min). The free PSS was removed with centrifugation (11,000 rpm, 15 min). Finally, 0.6 g of PDDAC was added and the same modification method as that used for PSS was applied. Additionally, a GO/GNR-iohexol solution was prepared by sonicating with 150 μL commercial iohexol (370 mg/mL).

2.4 Characterization

The morphology and structure of the GO/GNRs hybrids were characterized using a transmission electron microscope (TEM) (JEM-1230, Japan), a scanning electron microscope (SEM) (S-4800, Japan), X-ray photoelectron spectroscopy (XPS) (Axis Ultra DLD, Japan), and an atomic force microscope (AFM) (Bruker, USA). Modified GO/GNRs were measured from the visible to near-infrared light region by using ultraviolet–visible (UV–Vis) spectroscopy (Cary50, Varian). The thermogravimetric change of the GO/GNRs was measured with a thermogravimetric-differential thermal analysis (TG-DTA) simultaneous thermal analysis system (Netzsch, Germany). The zeta potential of the materials was determined using a dynamic light scattering system (Zeta Sizer Nano ZS90, Malvern) and the photothermal effect was monitored with an infrared thermal camera (Flir). The concentration of the GO/GNRs was measured with an inductive coupled plasma spectrometer (Hitachi Limited, Japan).

2.5 *In vitro* photothermal heating experiments

To measure the photostability and photothermal effect, solutions (1 mL) with different concentrations (0–50 μg/mL) of GO/GNRs were placed in 1.5-mL Eppendorf tubes and irradiated with an 808-nm NIR laser with a power density of 0.4 W/cm^2 for 6 min. The 50 μg/mL GO/GNR solution was irradiated for six on/off laser cycles. The temperature of the solutions was measured by an infrared thermal camera and the TEM and UV–Vis data of the irradiated sample were then obtained.

2.6 *In vitro* cytotoxicity test and photothermal ablation of cancer cells

The cytotoxicity of the GO/GNRs was tested using SW1990 cancer cells provided by Changhai Hospital (Shanghai, China). The cells were cultured in Dulbecco's modified Eagle medium (DMEM) containing 10% fetal bovine serum (FBS), 1% penicillin, and streptomycin at 37 ℃ and with 5% CO_2 for several weeks. The cells were then seeded overnight in a 96-well plate with a density of 1 × 10^4 cells per well. After the overnight culture, which improved the attachment of the cells attached, the medium was removed and substituted with fresh medium containing a different concentration of GO/GNR nanohybrids (0–100 μg/mL) and then incubated for 24 h. The cell viability was measured by a CCK-8 assay; 100 μL of CCK-8 in DMEM (V(CCK-8):V(DMEM) = 1:10) was added to each well and the cells were incubated for 3 h. The absorbance at 450 nm was recorded by a Thermo Scientific Multiskan MK3 ELISA reader according to the manufacturer's instructions.

The steps of the cell culture and seeding process were similar to those of the cytotoxicity test. The cells were incubated with the GO/GNRs for 12 h. Subsequently, the cells were washed three times with phosphate buffer solution (PBS) and cultured with fresh DMEM. Immediately, the cells were irradiated with an NIR laser (808 nm, 0.8 W/cm^2) for 10 min. Next, the cells were incubated for 24 h. The relative viability was measured using the CCK-8 assay.

2.7 *In vitro* and *in vivo* X-ray CT imaging

A series of aqueous solutions of GO/GNRs (0, 0.01, 0.025, 0.05, and 0.0638 M) were prepared. The CT imaging was monitored by a Siemens CT Sensation Cardiac 64 system with parameters 120 kVp, 240 mA, and a 512 × 512 matrix. To perform *in vivo* CT imaging, tumor-bearing nude mice were firstly anesthetized with 5% chloral hydrate and scanned with the CT scanner pre- and post-injection. GO/GNRs or GO/GNRs-iohexol (0.0683 M, 50–80 μL) were injected intratumorally. The *in vivo* CT imaging was performed using a GammaMedical X-CT/XO system with tube voltage 70 kVp, tube current 175 μA, and a 1,024 × 1,024 matrix.

2.8 *In vivo* PTT

Nude mice (four weeks old, female) were purchased from Shanghai Lab Animal Research Center and raised in Tongji University Lab Animal Research. After two weeks, pieces of a SW1990 tumor were planted. When the tumor size reached an average size of 100 mm^3, GO/GNRs (80–100 μL, 6.5 mM) and PBS were administered intratumorally. After injection, the tumors were immediately irradiated with the 808-nm laser at a power density of 0.3–0.4 W/cm^2 for 10 min. Meanwhile, thermal images of the tumors were recorded with an infrared thermal camera. The PTT processes were further observed by recording the tumor volumes and body weights. The tumor volumes (V) were determined using the equation $V = ab^2/2$.

2.9 Histological evaluation of organ toxicity

To evaluate the organ toxicity of the GO/GNRs *in vivo*, female nude mice were intravenously injected with 100 μL of the GO/GNRs (0.026 M). The control group was injected with 100 μL of PBS. After one month, the hearts, livers, spleens, lungs, and kidneys were harvested, washed with PBS, and immediately fixed with 4% buffered formalin solution. After fixation, the organs were processed, sectioned, and hematoxylin- and eosin-(H&E) stained for optical microscopic observation by technicians in Shanghai East Hospital (Shanghai, China).

3 Results and discussion

3.1 Preparation of GO/GNRs

Scheme 1 demonstrates the preparation process of the GO/GNR nanohybrids. Based on the zeta potential data of the GO and gold seeds, the negative charge of the GO must be improved to strengthen the connection between them. PSS molecules can not only improve the water solubility and biocompatibility of GO but also help prevent the aggregation of single GO layers because they provide adequate electrons (Fig. 1(d)). Sonicating at high power can simultaneously break GO into small pieces and noncovalently modify it with PSS. Meanwhile, a large number of GO/GNR nanohybrids were prepared by increasing the reactant ratio based on the preparation of the GO/GNRs nanohybrids. The growth of GNRs on GO-PSS has many advantages, including favorable distribution on the GO-PSS, a firm connection with GO-PSS, and photothermal stability. Additionally, PSS and PDDAC modifiers are inexpensive, water soluble, and biocompatible with abundant negative and positive charges, respectively, and they are widely used in biomedicine. Most importantly, both molecules are safe and nontoxic. PSS and PDDAC have also been investigated as modifiers to improve the toxicity of GNRs [42]. The GO/GNRs were firstly modified with PSS; PSS molecules were primarily attached on the surfaces of the GO/GNRs like a net to hinder the separation of surfactant CTAB from the surface of the GO/GNRs. To further consolidate this net, PDDAC molecules were used. The two-step modification was performed simply by ultrasonication.

3.2 Characterization

The SEM image of Fig. 1(a) shows well-stabilized GNRs on the surface of the GO-PSS. As displayed in

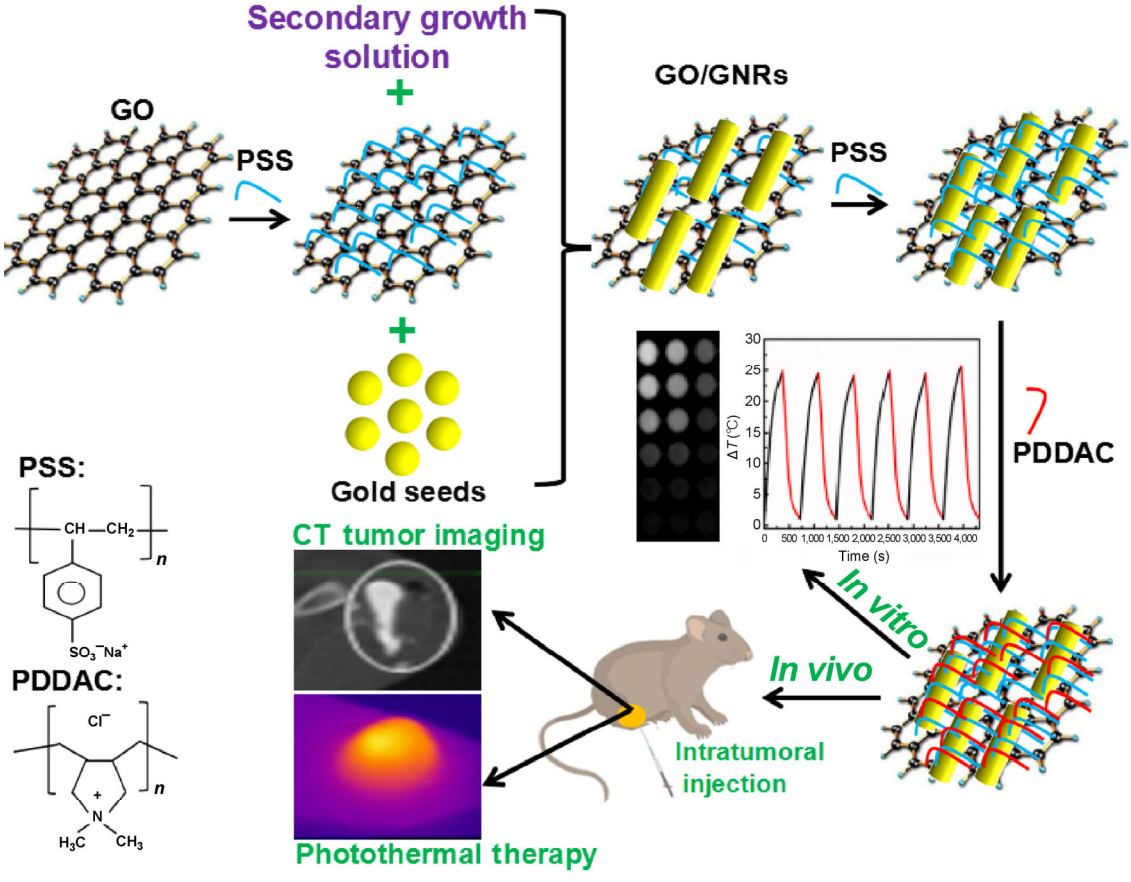

Scheme 1 Schematic illustration of the preparation and application of the GO/GNR hybrids.

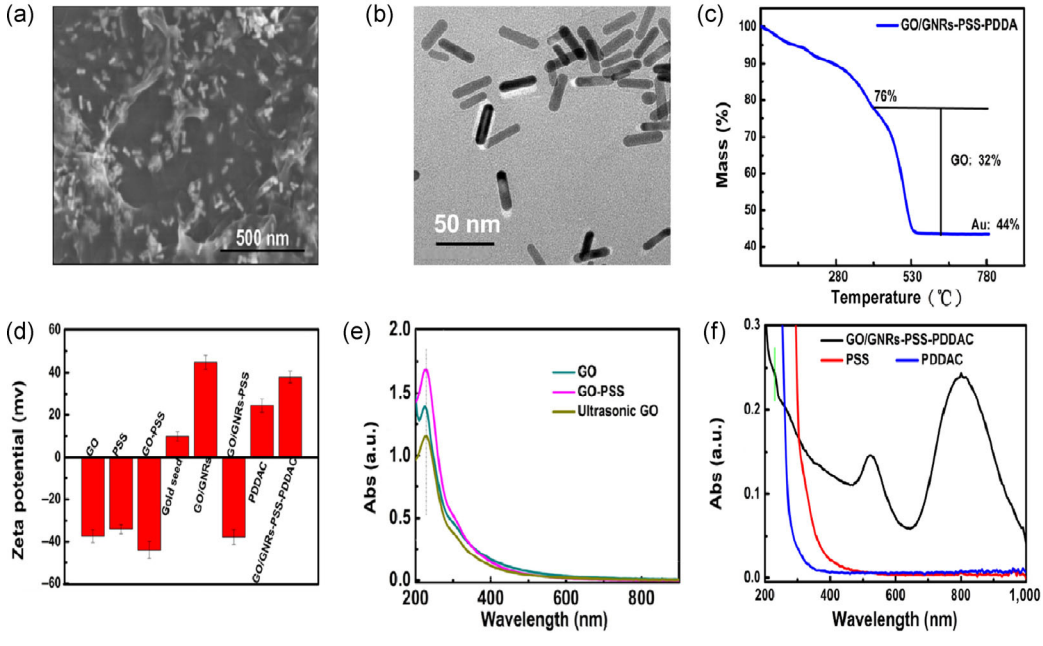

Figure 1 SEM (a), TEM (b), and TG-DTA (c) measurement results of GO/GNRs. Zeta potential of GO, PSS, GO-PSS, gold seeds, GO/GNRs, GO/GNRs-PSS, PDDAC, and GO/GNRs-PSS-PDDAC (d). UV–Vis spectra of GO, GO-PSS, and ultrasonic GO (e). UV–Vis spectra of PSS, PDDAC, and GO/GNRs-PSS-PDDAC (f).

Fig. 1(b), the average size of the GNRs is approximately 31 nm × 8 nm on a few layers of GO. Figure 1(a) also demonstrates that the GNRs are incorporated compactly into the soft template of the GO-PSS with a high productivity of GNRs on the GO-PSS. The TG-DTA result (Fig. 1(c)) shows a GO:GNR weight ratio of 0.727, which is consistent with the calculated quality of the reactant. Different weight ratios of GO:GNRs were produced by changing the amount of GO and thus modifying the density distribution of the GNRs on the GO-PSS (Fig. S1 in the Electronic Supplementary Material (ESM)). The zeta potentials of the gold seeds and GO-PSS were determined to be 10.1 and −44.7 mV. The growth process of the GO/GNRs began with gold seeds adhering on the GO-PSS through the electrostatic interaction and continued with the growth of the gold seeds into GNR on the GO-PSS. Although many studies have reported on the formation mechanism of GNRs [6, 43, 44], their conclusions differ considerably. As shown in Fig. 1(e), the UV–Vis absorption spectra of different GO samples are similar and exhibit a broad peak at 230 nm, and the absorption of the GO/GNR nanohybrids is neither red- nor blue-shifted at 230 nm, indicating un-reduced GO. In addition, the GO/GNRs show excellent absorption at 808 nm.

The AFM images show that GO-PSS has a smoother surface than the nonmodified GO. The GO-PSS surface appears to be snowflake-like, considerably different from those shown in Figs. 2(a) and 2(b). This can be explained by the homogeneous attachment of PSS onto the GO. Furthermore, the AFM cross-sectional images indicate a GO thickness of 1.0 nm and a GO-PSS height of 1.3 nm. The topography of the GO/GNR nanohybrids significantly changes (Fig. 2(d)) owing to the presence of GNRs on the GO-PSS. The cross-sectional view shows both the modifier PSS and PDDAC beside the GNRs. Moreover, the XPS spectra provide further information on the four examples regarding the increased C–C content (284.6 eV) and reduced C–O (286.8 eV) and C=O contents. These results indicate no chemical reaction between the GO and the PSS adsorbed on the GO through π–π stacking interactions. Figure S2 in the ESM shows two peaks of the Au 4f spectrum with binding energies 83.4 and 87.1 eV, which are consistent with the Au^0 state values 84.0 and 87.7 eV for Au $4f_{7/2}$ and Au $4f_{5/2}$, respectively, according to the XPS handbook.

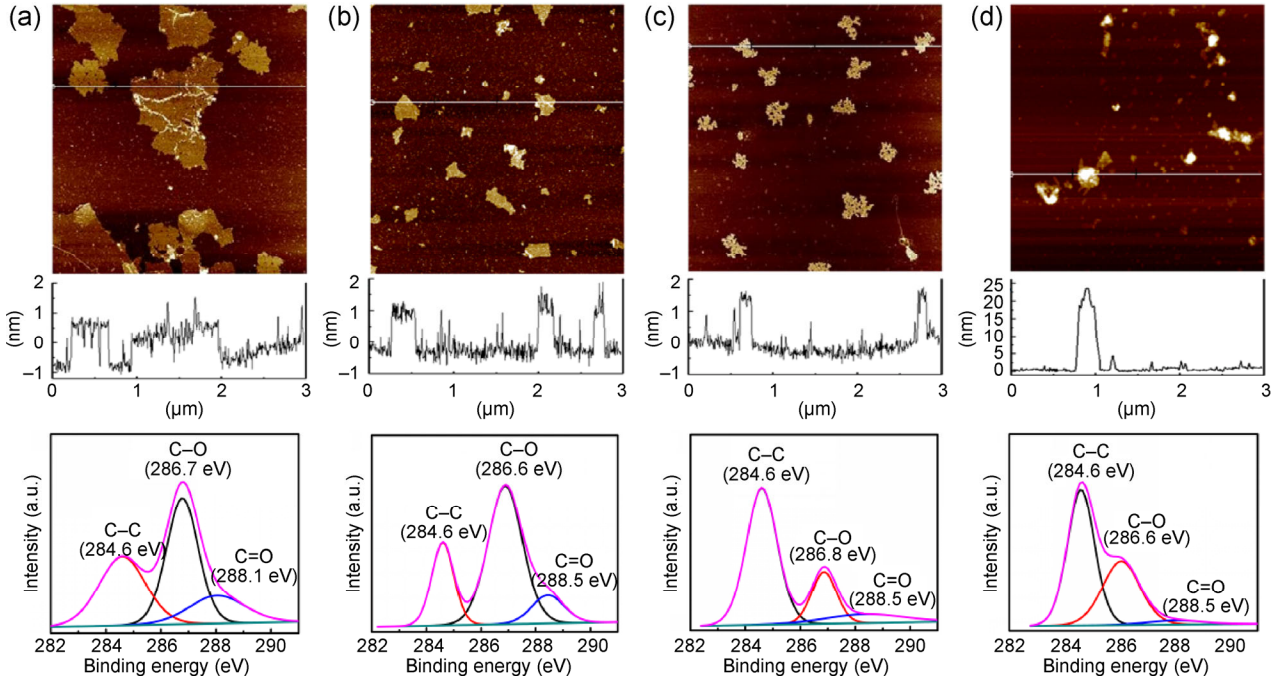

Figure 2 AFM images and XPS analysis of GO (a), ultrasonic GO (b), GO-PSS (c), and GO/GNRs (d).

3.3 *In vitro* photothermal effects of GO/GNRs

Compared with individual GNRs or GO, the GNRs mixed with the GO solution showed a stronger photothermal effect, as reported by Abdallah et al. [26]. Figure S3 in the ESM shows that GNRs (1) were prepared under identical fabrication conditions as the GO/GNR hybrids except the presence of GO. GNRs (2) were prepared by changing the amount of gold seeds and the resulting GO/GNR hybrids exhibited an enhanced photothermal effect compared to GNRs (1) and GNRs (2). This could be explained as follows. The large surface area and good electric and thermal conduction properties of GO can enhance heat transfer, hence avoiding local overheating. By shortening the distance between the GO and GNRs, the GO can serve as both a photothermal agent and a better conductor. To measure the photothermal effect of the GO/GNR nanohybrids, 0, 25, 35, and 50 μg/mL GO/GNRs were irradiated with an 808-nm laser (0.4 W/cm^2). Figure 3(a) shows the temperature variation of the GO/GNR nanohybrids upon the 808-nm laser irradiation, as acquired by an infrared thermal camera. As shown in Fig. 3(b), the temperature increases from 25 to 49.9 °C at a concentration of 50 μg/mL after 6 min of irradiation. Figure 3(c) shows the photothermal effect in a cyclic fashion at a concentration of 50 μg/mL for six on/off cycles of NIR-laser irradiation. The GO/GNR nanohybrids display an external photothermal effect stability. Figures 3(d)–3(f) display the results of the morphology and UV–Vis absorption measurements of the GO/GNRs before or after six cycles of laser irradiation. As shown in these figures, the laser irradiation cycle tests did not damage the character and morphology of the GO/GNRs. Thus, to some extent, the thermal stability of the GO/GNRs can increase their functionality at higher temperatures.

After centrifuging twice, most of the CTAB on the GO/GNRs was removed. The GO/GNR nanohybrids were positively charged and the zeta potential was approximately 47.2 mV. To reduce the toxicity of CTAB, PSS was used to modify the GO/GNRs through the electrostatic interaction. PSS, which has a negative charge and long chain, can easily connect with GO/GNRs but not detach from them. These advantages of PSS obstruct the removal of the remaining CTAB. The modification of the GO/GNRs-PSS results in a reversed zeta potential of −37.8 mV (Fig. 1(d)). To further lower the toxicity of the GO/GNR hybrids,

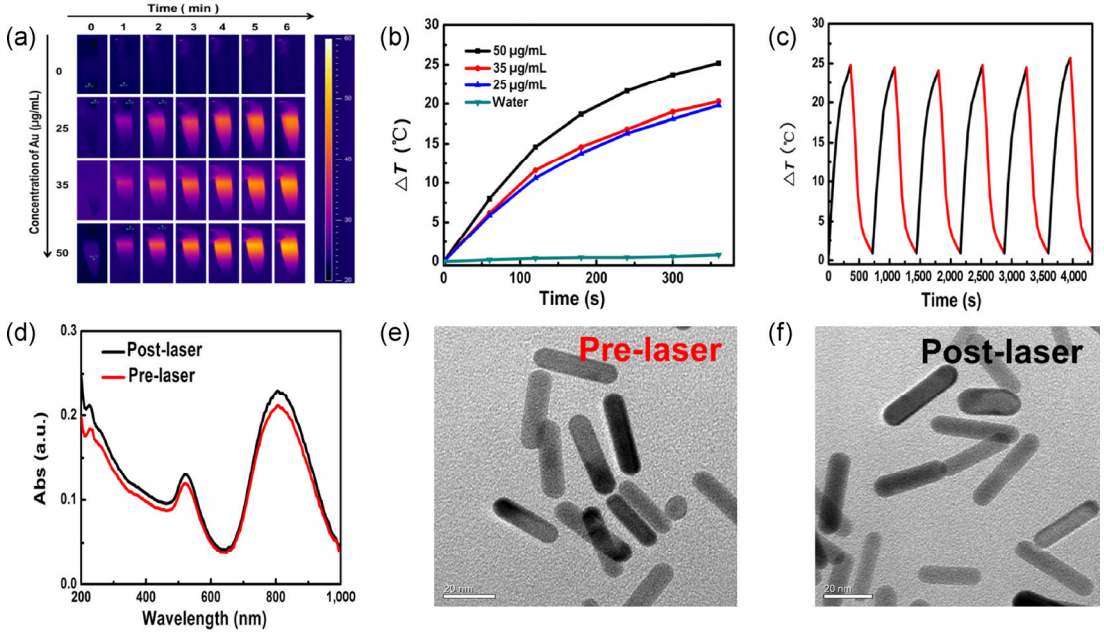

Figure 3 *In vitro* photothermal experiments. Real-time thermal imaging (a) and temperature profiles for different concentrations of GO/GNRs (b). Temperature variations of GO/GNRs (50 μg/mL) under continuous irradiation with an 808-nm laser for six cycles (c). UV–Vis spectra obtained before and after six cycles of irradiation (d). TEM images acquired before (e) and after (f) six cycles of laser irradiation (0.4 W/cm^2).

PDDAC with a positive charge was applied and the GO/GNRs-PSS-PDDAC showed low toxicity at a concentration of 100 μg/mL (based on Au) (Fig. 4(b)).

Using the procedure described in Ref. [1], the laser power density was reduced to reduce the damage to normal cells; however, the GO/GNRs still had good photothermal toxicity to SW1990 cancer cells. The SW1990 cells were cultured with a medium containing 0, 35, and 50 μg/mL of GO/GNRs (808 nm, 10 min, 0.8 W/cm^2). The cell viability sharply decreased after laser irradiation. Figure 4(b) shows that the photothermal cytotoxicity of the GO/GNRs resulted in killing more than 60% of the SW1990 cancer cells compared to 6%–8% when using only laser irradiation. The total cell killing rates reached more than 80%. These results indicate the great potential of GO/GNRs as photothermal agents.

3.4 *In vitro* and *in vivo* CT imaging of GO/GNRs

To explore the CT imaging potential of GO/GNRs, different concentrations of the three materials were monitored by X-ray CT. The commercial X-ray imaging agent iohexol was used as the control. Although clinical CT contrast agents provide good CT images, small molecules lead to quick excretion and short circulation. Recently, there has been much interest in the use of Au NPs as CT contrast agents to achieve better imaging effects [15–18]. Figure 5(b) shows the slopes of the three samples (iohexol, GO/GNRs, GO/GNRs-iohexol) that have a ratio of 2.29:1.79:1. The GO/GNRs were observed to be superior compared to commercial iohexol with the same molarity. Meanwhile, the GO/GNRs were successfully used as carriers for the small molecule iohexol, showing enhanced CT

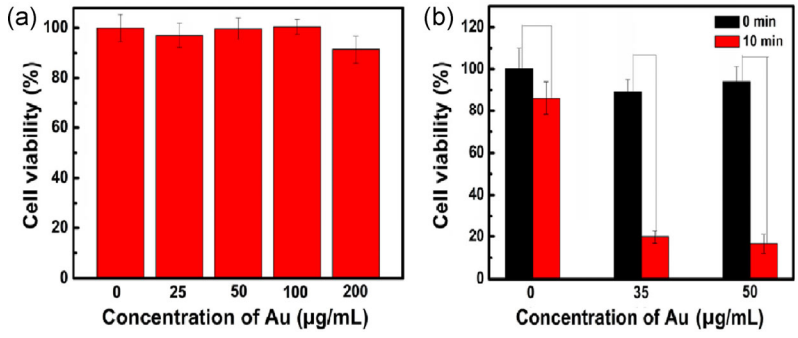

Figure 4 Cell viabilities of GO/GNR solutions with various Au concentrations (n = 3) (a). Cytotoxicity assay of SW1990 cells in the presence of different amounts of GO/GNRs with or without laser irradiation (808 nm) for 10 min (n = 3) (0.8 W/cm^2) (b).

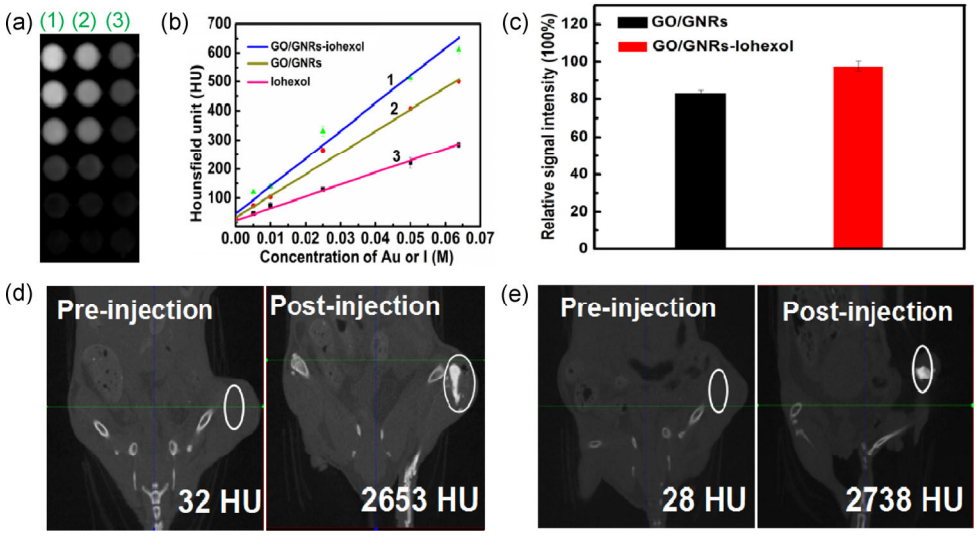

Figure 5 *In vitro* CT image (a) and X-ray attenuation intensity of (1) GO/GNRs-iohexol (based on Au), (2) GO/GNRs (based on Au), and (3) iohexol (based on I) as a function of the molar concentration of the radiodense element (b). Relative hounsfield unit (HU) signal before and after the intratumoral injection (c). CT imaging results for a tumor-bearing mouse before and after intratumoral injection with GO/GNRs (0.068 M, 50–80 μL) (d) and GO/GNRs-iohexol (0.068 M, 50–80 μL) (e).

imaging properties both *in vitro* and *in vivo*.

In vivo CT experiments were further performed by intratumoral injection of GO/GNR (Fig. 5(d)) (0.068 M, 50–80 μL) and GO/GNRs-iohexol (Fig. 5(e)) (0.068 M, 50–80 μL) solutions into the tumor-bearing nude mice. Figure 5(c) indicates that the Hounsfield unit signals obtained after the injection of the GO/GNRs and of GO/GNRs-iohexol are significantly brighter than that measured before the injection (100%). These results show that GO/GNRs are effective CT contrast agents and provide a versatile platform for functional iohexol molecules. These findings suggest that not only could GO/GNRs be used for excellent CT imaging, but also as a platform for iohexol and potentially as a highly desirable template for other functional molecules and NPs in medical imaging and therapy.

3.5 *In vivo* photothermal effect of GO/GNRs on the xenograft tumor model

To further examine PTT *in vivo*, the tumor-bearing nude mice received an intratumoral injection and were immediately exposed to an 808-nm laser of low laser power density (0.3–0.4 W/cm^2) for 10 min. The temperature changes at the tumor site were monitored with an infrared thermal camera. Photothermal agents with photostability contribute to PTT with an adjustable laser exposure time and steady tumor ablation temperature. Figure 6(a) shows that after intratumoral injection with GO/GNRs (80–100 μL,

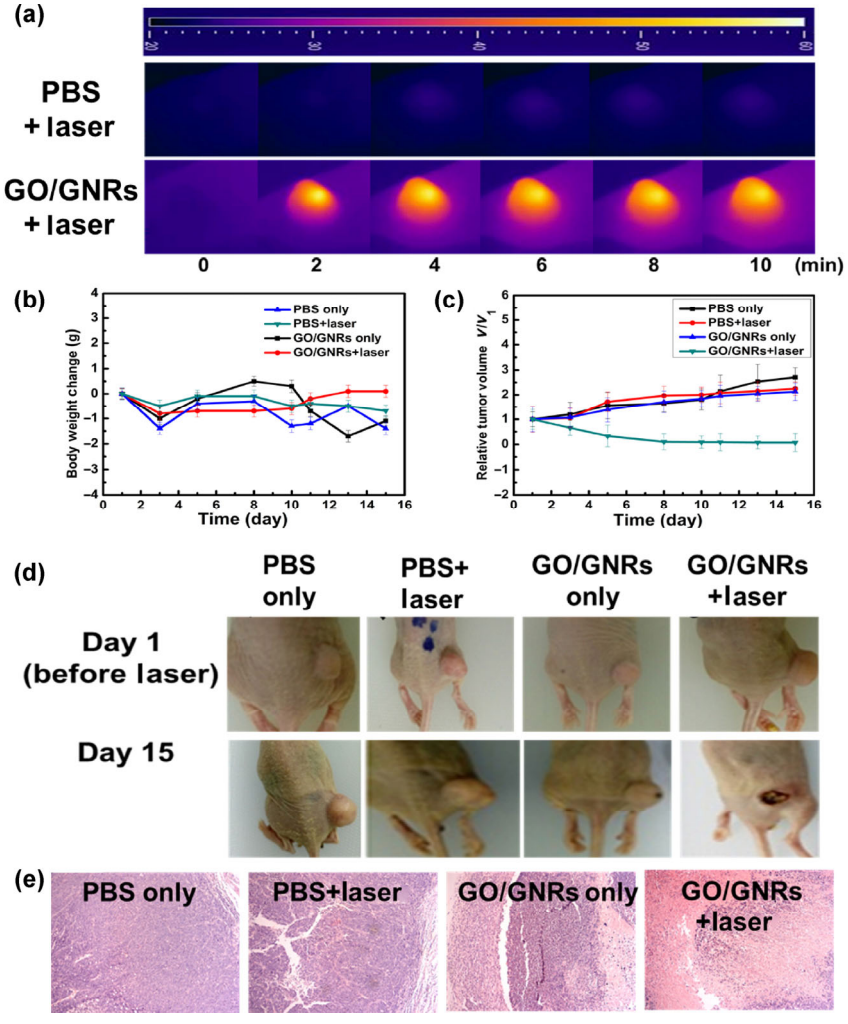

Figure 6 *In vivo* PTT. Real-time thermal image of SW1990-tumor-bearing mice after intratumoral injection with PBS and GO/GNRs (80–100 μL, 6.5 mM, 0.3–0.4 W/cm^2) (a). Body weight changes (b) and relative tumor volume (c) of the tumor-bearing mice after intratumoral injection with PBS and GO/GNRs. Images of nude mice before and after treatment (d). Image (original magnification × 10^5) of H&E-stained tumor sections harvested from tumor-bearing mice treated with PBS and GO/GNRs with or without laser irradiation (e).

6.5 mM), the tumor temperature increases rapidly from 24.8 to 59.7 ℃. The tumor volume and body weight changes were calculated from the beginning of the treatment (Figs. 6(b) and 6(c)) and no obvious weight change was detected. After the intratumoral injection of GO/GNRs, the tumor reduced rapidly (Fig. S4 in the ESM) but the injection of the controls (PBS only, PBS-laser, and GO/GNRs only) did not show the same effect. The tumor-bearing nude mice that were intratumorally injected with GO/GNRs were nearly healed within 15 days (Fig. 6(d)). After 15 days, the pathological changes in the tumors were determined by H&E staining, which showed cancer cell apoptosis in the experimental groups. The four groups confirmed that the GO/GNRs were effective in tumor killing at low-power laser density.

3.6 Histological evaluation of organ toxicity

One month after the intravenous injection, the pathological changes in several major organs were determined by H&E staining. The GO/GNRs did not appear to be toxic to normal organs (Fig. 7). The long-term toxicity assessment of the GO/GNRs showed no obvious inflammation, cell necrosis, or apoptosis.

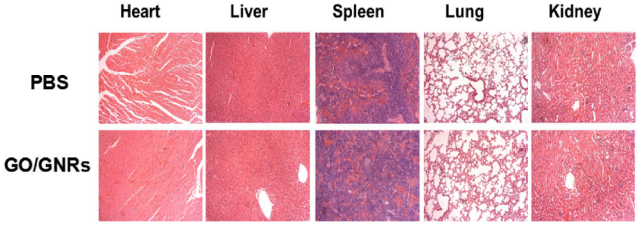

Figure 7 Histological images (original magnification × 10^5) of the heart, liver, spleen, lung, and kidney of the mice, obtained one month after intravenous injection with GO/GNRs (0.026 M, 100 μL). Mice injected with 100 μL of PBS were used as the control group. The examined organ sections were H&E-stained and observed under an optical microscope.

4 Conclusions

GO/GNR hybrids were synthesized using a GO- and gold-seed-mediated *in situ* growth method at room temperature. This *in situ* synthesis is highly adaptable for developing other types of GO/NPs. The GO/GNRs were successfully used as a versatile carrier of the small molecule iohexol for enhanced CT tumor imaging. Moreover, the GO/GNR nanohybrids demonstrated excellent photostability over six laser irradiation cycles and localized tumor killing ability and have therefore great potential for application in precise CT-image-guided tumor PTT.

Acknowledgements

This work was financially supported by National Natural Science Foundation of China (No. 51302190), Shanghai Natural Science Foundation (No. 16ZR1400700) and Shanghai Health and Family Planning Commission Project (Nos. 20144Y0248 and 2012y193). We are extremely grateful to Prof. Wei An (Tongji University) for great help with infrared thermal camera. We also thank Mr. Chengwei Shao (Changhai Hospital) for kind help with commercial iohexol and SW1990 tumor cells.

Electronic supplementary materials: Supplementary material (TEM of GO/GNRs with higher GO:GNRs weight ratio, XPS spectra of Au 4f, UV–Vis absorption spectra and PTT *in vitro* of GNRs and GO/GNRs, and image of PTT *in vivo* after three days) is available in the online version of this article at http://dx.doi.org/10.1007/s12274-016-1264-x.

References

[1] Choi, W. I.; Kim, J. Y.; Kang, C.; Byeon, C. C.; Kim, Y. H.; Tee, G. Tumor regression *in vivo* by photothermal therapy based on gold-nanorod-loaded, functional nanocarriers. *ACS Nano* **2011**, *5*, 1995–2003.

[2] Jang, B.; Park, J. Y.; Tung, C. H.; Kim, I. H.; Choi, Y. Gold nanorod-photosensitizer complex for near-infrared fluorescence imaging and photodynamic/photothermal therapy *in vivo*. *ACS Nano* **2011**, *5*, 1086–1094.

[3] Bagley, A. F.; Hill, S.; Rogers, G. S.; Bhatia, S. N. Plasmonic photothermal heating of intraperitoneal tumors through the use of an implanted near-infrared source. *ACS Nano* **2013**, *7*, 8089–8097.

[4] Wang, B. K.; Yu, X. F.; Wang, J. H.; Li, Z. B.; Li, P. H.; Wang, H. Y.; Song, L.; Chu, P. K.; Li, C. Z. Gold-nanorods-sirna nanoplex for improved photothermal therapy by gene silencing. *Biomaterials* **2016**, *78*, 27–39.

[5] Wang, N. N.; Zhao, Z. L.; Lv, Y. F.; Fan, H. H.; Bai, H. R.; Meng, H. M.; Long, Y. Q.; Fu, T.; Zhang, X. B.; Tan, W. H. Gold nanorod-photosensitizer conjugate with extracellular

pH-driven tumor targeting ability for photothermal/ photodynamic therapy. *Nano Res.* **2014**, *7*, 1291–1301.

[6] Nikoobakht, B.; El-Sayed, M. A. Preparation and growth mechanism of gold nanorods (NRs) using seed-mediated growth method. *Chem. Mater.* **2003**, *15*, 1957–1962.

[7] Busbee, B. D.; Obare, S. O.; Murphy, C. J. An improved synthesis of high-aspect-ratio gold nanorods. *Adv. Mater.* **2003**, *15*, 414–416.

[8] Xiao, Y. L.; Hong, H.; Matson, V. Z.; Javadi, A.; Xu, W. J.; Yang, Y. A.; Zhang, Y.; Engle, J. W.; Nickles, R. J.; Cai, W. B. et al. Gold nanorods conjugated with doxorubicin and cRGD for combined anticancer drug delivery and PET imaging. *Theranostics* **2012**, *2*, 757–768.

[9] Huang, H. C.; Barua, S.; Kay, D. B.; Rege, K. Simultaneous enhancement of photothermal stability and gene delivery efficacy of gold nanorods using polyelectrolytes. *ACS Nano* **2010**, *4*, 1769–1770.

[10] Parab, H. J.; Chen, H. M.; Lai, T.-C.; Huang, J. H.; Chen, P. H.; Liu, R.-S.; Hsiao, M.; Chen, C.-H.; Tsai, D.-P.; Hwu, Y.-K. Biosensing, cytotoxicity, and cellular uptake studies of surface-modified gold nanorods. *J. Chem. Phys. C* **2009**, *113*, 7574–7578.

[11] Apte, A.; Bhaskar, P.; Das, R.; Chaturvedi, S.; Poddar, P.; Kulkarni, S. Self-assembled vertically aligned gold nanorod superlattices for ultra-high sensitive detection of molecules. *Nano Res.* **2015**, *8*, 907–919.

[12] Jokerst, J. V.; Cole, A. J.; Van de Sompel, D.; Gambhir, S. S. Gold nanorods for ovarian cancer detection with photoacoustic imaging and resection guidance via Raman imaging in living mice. *ACS Nano* **2012**, *6*, 10366–10377.

[13] Huang, X. H.; El-Sayed, I. H.; Qian, W.; El-Sayed, M. A. Cancer cell imaging and photothermal therapy in the near-infrared region by using gold nanorods. *J. Am. Chem. Soc.* **2006**, *128*, 2115–2120.

[14] He, W.; Henne, W. A.; Wei, Q. S.; Zhao, Y.; Doorneweerd, D. D.; Cheng, J.-X.; Low, P. S.; Wei, A. Two-photon luminescence imaging of bacillus spores using peptide-functionalized gold nanorods. *Nano Res.* **2008**, *1*, 450–456.

[15] Dou, Y.; Guo, Y. Y.; Li, X. D.; Li, X.; Wang, S.; Wang, L.; Lv, G. X.; Zhang, X. N.; Wang, H. J.; Gong, X. Q. et al. Size-tuning ionization to optimize gold nanoparticles for simultaneous enhanced CT imaging and radiotherapy. *ACS Nano* **2016**, *10*, 2536–2548.

[16] Meir, R.; Shamalov, K.; Betzer, O.; Motiei, M.; Horovitz-Fried, M.; Yehuda, R.; Popovtzer, A.; Popovtzer, R.; Cohen, C. J. Nanomedicine for cancer immunotherapy: Tracking cancer-specific T-cells *in vivo* with gold nanoparticles and CT imaging. *ACS Nano* **2015**, *9*, 6363–6372.

[17] Zhang, J. M.; Li, C.; Zhang, X.; Huo, S. D.; Jin, S. B.; An, F. F.; Wang, X. D.; Xue, X. D.; Okeke, C. I.; Duan, G. Y. et al. *In vivo* tumor-targeted dual-modal fluorescence/CT imaging using a nanoprobe co-loaded with an aggregation-induced emission dye and gold nanoparticles. *Biomaterials* **2015**, *42*, 103–111.

[18] Zhang, Y. X.; Wen, S. H.; Zhao, L. Z.; Li, D.; Liu, C. C.; Jiang, W. B.; Gao, X.; Gu, W. T.; Ma, N.; Zhao, J. H. et al. Ultrastable polyethyleneimine-stabilized gold nanoparticles modified with polyethylene glycol for blood pool, lymph node and tumor CT imaging. *Nanoscale* **2016**, *8*, 5567–5577.

[19] Zhang, W.; Guo, Z. Y.; Huang, D. Q.; Liu, Z. M.; Guo, X.; Zhong, H. Q. Synergistic effect of chemo-photothermal therapy using PEGylated graphene oxide. *Biomaterials* **2011**, *32*, 8555–8561.

[20] Yang, K.; Zhang, S. A.; Zhang, G. X.; Sun, X. M.; Lee, S. T.; Liu, Z. A. Graphene in mice: Ultrahigh *in vivo* tumor uptake and efficient photothermal therapy. *Nano Lett.* **2010**, *10*, 3318–3323.

[21] Robinson, J. T.; Tabakman, S. M.; Liang, Y. Y.; Wang, H. L.; Casalongue, H. S.; Vinh, D.; Dai, H. J. Ultrasmall reduced graphene oxide with high near-infrared absorbance for photothermal therapy. *J. Am. Chem. Soc.* **2011**, *133*, 6825–6831.

[22] Liu, Z.; Robinson, J. T.; Sun, X. M.; Dai, H. J. PEGylated nanographene oxide for delivery of water-insoluble cancer drugs. *J. Am. Chem. Soc.* **2008**, *130*, 10876–10877.

[23] Sun, X. M.; Liu, Z.; Welsher, K.; Robinson, J. T.; Goodwin, A.; Zaric, S.; Dai, H. J. Nano-graphene oxide for cellular imaging and drug delivery. *Nano Res.* **2008**, *1*, 203–212.

[24] Zhou, X.; Laroche, F.; Lamers, G. E. M.; Torraca, V.; Voskamp, P.; Lu, T.; Chu, F. Q.; Spaink, H. P.; Abrahams, J. P.; Liu, Z. F. Ultra-small graphene oxide functionalized with polyethylenimine (PEI) for very efficient gene delivery in cell and zebrafish embryos. *Nano Res.* **2012**, *5*, 703–709.

[25] Ma, X. X.; Tao, H. Q.; Yang, K.; Feng, L. Z.; Cheng, L.; Shi, X. Z.; Li, Y. G.; Guo, L.; Liu, Z. A functionalized graphene oxide-iron oxide nanocomposite for magnetically targeted drug delivery, photothermal therapy, and magnetic resonance imaging. *Nano Res.* **2012**, *5*, 199–212.

[26] Zedan, A. F.; Moussa, S.; Terner, J.; Atkinson, G.; El-Shall, M. S. Ultrasmall gold nanoparticles anchored to graphene and enhanced photothermal effects by laser irradiation of gold nanostructures in graphene oxide solutions. *ACS Nano* **2013**, *7*, 627–636.

[27] Moon, H.; Kumar, D.; Kim, H.; Sim, C.; Chang, J. H.; Kim, J. M.; Kim, H.; Lim, D. K. Amplified photoacoustic performance and enhanced photothermal stability of reduced graphene oxide coated gold nanorods for sensitive photoacoustic imaging. *ACS Nano* **2015**, *9*, 2711–2719.

[28] Turcheniuk, K.; Hage, C. H.; Spadavecchia, J.; Heliot, L.;

Boukherroub, R.; Szunerits, S. Plasmonic photothermal therapy with gold nanorods/reduced graphene oxide core/shell nanocomposites. In *Encyclopedia of Nanotechnology*; Bhushan, B., Ed.; Springer: Netherlands, 2015; pp 1–8.

[29] Song, J. B.; Yang, X. Y.; Jacobson, O.; Lin, L. S.; Huang, P.; Niu, G.; Ma, Q. J.; Chen, X. Y. Sequential drug release and enhanced photothermal and photoacoustic effect of hybrid reduced graphene oxide-loaded ultrasmall gold nanorod vesicles for cancer therapy. *ACS Nano* **2015**, *9*, 9199–9209.

[30] Dembereldorj, U.; Choi, S. Y.; Ganbold, E. O.; Song, N. W.; Kim, D.; Choo, J.; Lee, S. Y.; Kim, S.; Joo, S. W. Gold nanorod-assembled pegylated graphene-oxide nanocomposites for photothermal cancer therapy. *Photochem. Photobiol.* **2014**, *90*, 659–666.

[31] Goncalves, G.; Marques, P. A. A. P.; Granadeiro, C. M.; Nogueira, H. I. S.; Singh, M. K.; Grácio, J. Surface modification of graphene nanosheets with gold nanoparticles: The role of oxygen moieties at graphene surface on gold nucleation and growth. *Chem. Mater.* **2009**, *21*, 4796–4802.

[32] Huang, J.; Zhang, L. M.; Chen, B. A.; Ji, N.; Chen, F. H.; Zhang, Y.; Zhang, Z. J. Nanocomposites of size-controlled gold nanoparticles and graphene oxide: Formation and applications in SERS and catalysis. *Nanoscale* **2010**, *2*, 2733–2738.

[33] Xu, C.; Yang, D. R.; Mei, L.; Li, Q. H.; Zhu, H. Z.; Wang, T. H. Targeting chemophotothermal therapy of hepatoma by gold nanorods/graphene oxide core/shell nanocomposites. *ACS Appl. Mater. Interfaces* **2013**, *5*, 12911–12920.

[34] Jin, Y. S.; Wang, J. R.; Ke, H. T.; Wang, S. M.; Dai, Z. F. Graphene oxide modified PLA microcapsules containing gold nanoparticles for ultrasonic/CT bimodal imaging guided photothermal tumor therapy. *Biomaterials* **2013**, *34*, 4794–4802.

[35] Shi, J. J.; Wang, L.; Zhang, J.; Ma, R.; Gao, J.; Liu, Y.; Zhang, C. F.; Zhang, Z. Z. A tumor-targeting near-infrared laser-triggered drug delivery system based on GO@Ag nanoparticles for chemo-photothermal therapy and X-ray imaging. *Biomaterials* **2014**, *35*, 5847–5861.

[36] Chen, F.; Yang, Q.; Zhong, Y.; An, H. X.; Zhao, J. W.; Xie, T.; Xu, Q. X.; Li, X. M.; Wang, D. B.; Zeng, G. M. Photo-reduction of bromate in drinking water by metallic Ag and reduced graphene oxide (RGO) jointly modified $BiVO_4$ under visible light irradiation. *Water Res.* **2016**, *101*, 555–563.

[37] Shen, J. F.; Shi, M.; Li, N.; Yan, B.; Ma, H. W.; Hu, Y. Z.; Ye, M. X. Facile synthesis and application of Ag-chemically converted graphene nanocomposite. *Nano Res.* **2010**, *3*, 339–349.

[38] Hou, C. Y.; Quan, H. C.; Duan, Y. R.; Zhang, Q. H.; Wang, H. Z.; Li, Y. G. Facile synthesis of water-dispersible Cu_2O nanocrystal-reduced graphene oxide hybrid as a promising cancer therapeutic agent. *Nanoscale* **2013**, *5*, 1227–1232.

[39] Bai, J.; Liu, Y. W.; Jiang, X. E. Multifunctional PEG-GO/CuS nanocomposites for near-infrared chemo-photothermal therapy. *Biomaterials* **2014**, *35*, 5805–5813.

[40] Peng, C. X.; Chen, B. D.; Qin, Y.; Yang, S. H.; Li, C. Z.; Zuo, Y. H.; Liu, S. Y.; Yang, J. H. Facile ultrasonic synthesis of CoO quantum dot/graphene nanosheet composites with high lithium storage capacity. *ACS Nano* **2012**, *6*, 1074–1081.

[41] Marcano, D. C.; Kosynkin, D. V.; Berlin, J. M.; Sinitskii, A.; Sun, Z. Z.; Slesarev, A.; Alemany, L. B.; Lu, W.; Tour, J. M. Improved synthesis of graphene oxide. *ACS Nano* **2010**, *4*, 4806–4814.

[42] Wang, L. M.; Jiang, X. M.; Ji, Y. L.; Bai, R.; Zhao, Y. L.; Wu, X. C.; Chen, C. Y. Surface chemistry of gold nanorods: Origin of cell membrane damage and cytotoxicity. *Nanoscale* **2013**, *5*, 8384–8391.

[43] Edgar, J. A.; McDonagh, A. M.; Cortie, M. B. Formation of gold nanorods by a stochastic "popcorn" mechanism. *ACS Nano* **2012**, *6*, 1116–1125.

[44] Morita, T.; Tanaka, E.; Inagaki, Y.; Hotta, H.; Shingai, R.; Hatakeyama, Y.; Nishikawa, K.; Murai, H.; Nakano, H.; Hino, K. Aspect-ratio dependence on formation process of gold nanorods studied by time-resolved distance distribution functions. *J. Chem. Phys. C* **2010**, *114*, 3804–3810.